Preprints of the 21st IFAC World Congress (Virtual)
Berlin, Germany, July 12-17, 2020

Feedforward and H_∞ Feedback Robotic Force Control in a 1-dof Physical Interaction Using a Nonlinear Human Model

Mourad Benoussaad* and Micky Rakotondrabe

LGP-ENIT, Toulouse INP, University of Toulouse, Tarbes, France
* *corresponding author: mourad.benoussaad@enit.fr*

Abstract: Robot interacting with flexible object, and particularly with human in movement, is an increasing topic in several applications of today. It is particularly interesting and challenging in term of modeling and control because of the human variability, uncertainty and non-linearity. In the current work, we propose an original approach to model and control the interaction between a 1-dof robotic system and a human. While the human model includes a nonlinear biomechanical model, the nonlinearity is accounted and compensated for in a feedforward controller. Then a robust H_∞ feedback control is added in order to allow the closed-loop satisfy some specified performances under possible uncertainties and under external disturbance such as noise. The feedforward-feedback control is afterwards extensively verified in simulation which confirm its efficiency.

Keywords: Human-robotic interaction, modeling, nonlinear feedforward control, H_∞ feedback control, 1-dof

1. INTRODUCTION

Interaction and manipulation in unknown environment is a challenging robotic task with a rising complexity when a non-rigid or deformable object is in the loop. Deformable objects can be manifold: biological objects (organs, tissues and meat), human limbs, wire and cables, textile, fruit and vegetable, or some food and industrial products. Robotic manipulation of deformable objects includes several applications such as robotics for surgery and for butchery where robot should manipulate organs - biological tissues or meat, and collaborative robotics. In collaborative robotics, one can find robot-robot interaction with a deformable object between them [1, 2, 3, 4, 5], human-robot interaction with an object between them [6], and a direct human-robot interaction [7]. In all these cases, robotic manipulation of flexible objects should address several aspects [8, 9, 4, 10, 11]: studies of the end-effector (gripper or multi-fingered hand), studies of the sensing type (force, position) and of the measurement approach (force sensor, model-based measurement, vison-based measurement), and studies of the control.

Robotic control for deformable object manipulation involves many issues such as object nonlinear deformation and lack of object behavior knowledge. Unlike manipulation of rigid object which can be considered as a continuity of the robot end-effector, robotic manipulation of deformable object can be seen as an under-actuated system because the object deformation introduces additional degrees of freedom. Several control strategies have been previously explored with different types of feedback. A visual servoing based control law was suggested in [6, 12] and used the object image for the feedback. Simular approach was proposed in [13] but for a different application. To handle the issues of varying parameters and model uncertainty due to the deformation of the object, a robust control was employed in [3]. Most of these previous works do not fully consider the model of the deformable object in the control strategy. Nevertheless, in the case where there is no vision feedback and visual servoing available, it becomes mandatory to use a model of the deformable object and to consider this during the controller synthesis. Particularly, when the object presents a comparable mechanical impedance with respect to the robot, such as in human-robot interaction, the consideration of human model in the robotic control law seems an essential strategy.

This paper aims to explore the force control of robot interacting with a human body by including human nonlinear model. For that, a feedforward controller will be synthesized to compensate first for the nonlinearity. Then a robust H_∞ feedback control will be added to reach some specified performances under uncertainties and external disturbance. The current study contributions are: the introduction of a nonlinear human model to synthesize controller for human-robot interaction, and the design of a feedforward-feedback architecture for force control in a human-robot interaction. The paper uses a 1-dof robotic system for this preliminary result but future work will consider more common robot (6-dof) with more manipulation Cartesian axis and the experimental validation.

The remainder of the paper is organized as follow. In section-2, the whole system, i.e. human-robot interaction, is described and its model is established. In section-3, the robot force control design is detailed. Section-4 is devoted to simulation and related results discussed. Finally conclusion and perspectives of this work are summarized in section-5.

2. PRESENTATION OF THE ROBOTIC SYSTEM AND MODELING

2.1 Presentation of the platform

Fig.1 displays the platform which consists of a human in interaction and a one degree-of-freedom (1-dof) robotized system. The human is sitting on a chair, with tilted back and strapped shoulder in order to fix the upper part of the body. The lower part of the body is movable through knee in flexion thanks to the force applied by the robot. Finally, the feet are assumed to be tied on the extremity of the robot.

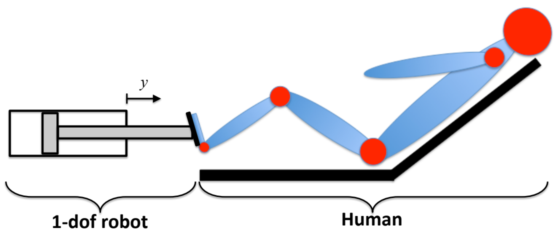

Fig. 1. Presentation of the human-robot in interaction.

The aim of this paper being to further control the force applied by the 1-dof robotic system, the next subsection will derive the force model of the human-robot interaction. In the sequel, we consider the human to be passive, i.e. he/she does not deliberately generate any force to the robot. This assumption is motivated by the considered application (relaxing exercise) or by similar case (massage).

2.2 Human-robot interaction modeling

In [14], a biomechanical human linear model was proposed. The model, usable when the entire body is in interaction with the environment, is a cascade of two mass-spring-damper subsystems each of which represents the lower and the upper parts. However, [15] raised the possible presence of hysteresis phenomenon in the behavior of the human without giving any explicit model. Thus, let us consider the scheme in Fig.2 to approximate the human-robot interaction of Fig.1. Furthermore, let us consider the robot as actuated by a linear motor of which the input control is a driving voltage $u(t)$. We assume that the robot model is of second order. This is motivated by the fact that the robot is much more rapid than the human and thus its first resonance is sufficient for the model. As a consequence, the governing equations are given by:

$$\begin{cases} m_1\ddot{x}_1 = F - h - c_1(\dot{x}_1 + \dot{x}_2) - k_1(x_1 - x_2) \\ m_2\ddot{x}_2 = h + c_1(\dot{x}_1 - \dot{x}_2) + k_1(x_1 - x_2) - c_2\dot{x}_2 - k_2x_2 \\ h = H_t(F) \\ y = x_1 \\ m_r\ddot{y} = au - F - c_r\dot{y} - k_r y \end{cases} \tag{1}$$

where the four first equations present the human behavior and the last equation presents the robot behavior. In these, x_1 and x_2 are the displacements of the human lower and upper parts respectively, y is the displacement of the robot extremity, F is the force applied by the robot, and $h(t) = H_t(F(t))$ is the result of the hysteresis in the human behavior such that $H_t(\cdot)$ is a hysteresis nonlinear operator. The names and numerical values of the different parameters, taken from [14] for the human model, are given in Table.1.

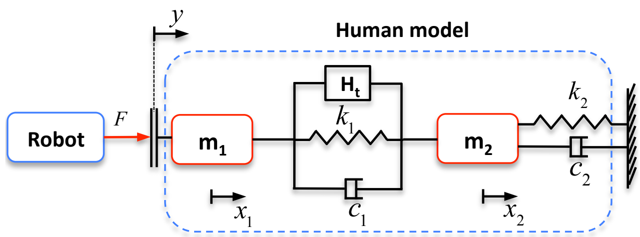

Fig. 2. Human body (flexible object) model interacting with robot.

Table 1. Numerical values.

Human lower part		
equivalent mass	m_1	$62[kg]$
equivalent damping coefficient	c_1	$810[Ns/m]$
equivalent stiffness	k_1	$8450[N/m]$
Human upper part		
equivalent mass	m_2	$10[kg]$
equivalent damping coefficient	c_2	$940[Ns/m]$
equivalent stiffness	k_2	$4520[N/m]$
Robotic system		
force to voltage ratio	a	$0.1[N/V]$
equivalent mass	m_r	$2[kg]$
equivalent damping coefficient	c_r	$5[Ns/m]$
equivalent stiffness	k_r	$10[N/m]$

Applying Laplace transform to the governing equations in Eq.1 and combining them, we derive the following relation between the force and the driving voltage:

$$F(s) - G_o(s) \cdot G_H \cdot h(s) = G_o(s) \cdot u(s) \tag{2}$$

$$\Leftrightarrow F(s) - G_o(s) \cdot G_H \cdot H(F(s)) = G_o(s) \cdot u(s) \tag{3}$$

where $h(s) = H(F(s))$ is the result of the hysteresis nonlinear operator $H(\cdot)$ when working in the Laplace domain ($H_t(F(t))$ being the time-domain operator), and where

$$\begin{cases} G_o(s) = \frac{\alpha_4 s^4 + \alpha_3 s^3 + \alpha_2 s^2 + \alpha_1 s + \alpha_0}{\beta_4 s^4 + \beta_3 s^3 + \beta_2 s^2 + \beta_1 s + \beta_0} \\ G_H(s) = \frac{\gamma_4 s^4 + \gamma_3 s^3 + \gamma_2 s^2 + \gamma_1 s + \gamma_0}{\alpha_4 s^4 + \alpha_3 s^3 + \alpha_2 s^2 + \alpha_1 s + \alpha_0} \end{cases} \tag{4}$$

with:

→ $\alpha_4 = am_1m_2$; $\alpha_3 = a(m_1(c_1 + c_2) + c_1m_2)$; $\alpha_2 = a(m_1(k_1 + k_2) + c_1c_2 + k_1m_2)$; $\alpha_1 = a(c_1k_2 + c_2k_1)$ and $\alpha_0 = ak_1k_2$;

→ $\beta_4 = \alpha_4 + m_rm_2$; $\beta_3 = \alpha_3 + m_r(c_1 + c_2) + c_rm_2$; $\beta_2 = \alpha_2 + m_r(k_1 + k_2) + c_r(c_1 + c_2) + k_rm_2$; $\beta_1 = \alpha_1 + c_r(k_1 + k_2) + k_r(c_1 + c_2)$ and $\beta_0 = \alpha_0 + k_r(k_1 + k_2)$;

$\rightarrow \gamma_4 = m_r m_2$; $\gamma_3 = m_r c_2 + c_r m_2$; $\gamma_2 = m_r k_2 + k_r m_2 + c_r c_2$; $\gamma_1 = c_r k_2 + k_r c_2$ and $\gamma_0 = k_r k_2$.

Because of the difficulty to extract $F(s)$ from Eq.3 due to the nonlinear operator $H(\cdot)$, let us suggest the following force extraction:

$$F(s) = G_o(s) \cdot (u(s) + G_H(s) \cdot H(F(s))) \tag{5}$$

It is clear that Eq.5 is non-causal because $F(s)$ is calculated as function of $F(s)$. Let us therefore rewrite Eq.5 as in Eq.6 where, instead of using $F(s)$ as argument, we use a different signal $F^-(s)$ to calculate the output $F(s)$, with $F^-(s)$ being the previous value of the force.

$$F(s) \approx G_o(s) \cdot \left(u(s) + G_H(s) \cdot H\left(F^-(s)\right)\right) \tag{6}$$

The block-diagram of the force model described by Eq.6 is given in Fig.3(a) which is equivalent to Fig.3(b). Both the two block diagrams indicate that the proposed force model has a structure called inverse multiplicative. Such structure could be very useful when synthesizing a feedforward control as we will see in the next section.

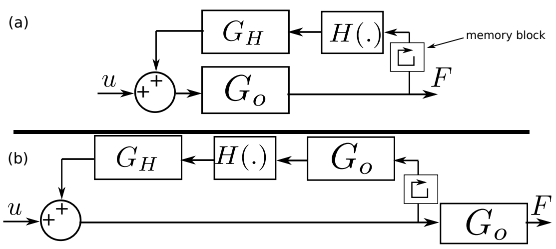

Fig. 3. Inverse multiplicative structured model.

3. FEEDFORWARD / H_∞ FEEDBACK FORCE CONTROL

In this section, the force model of Fig.3 will be used to calculate a feedback force control law. However, we suggest first a feedforward controller in order to compensate for the nonlinearity $H(\cdot)$ allowing afterwards the use of linear feedback controller design.

3.1 Feedforward control

Inverse multiplicative structure has been demonstrated in [16, 17, 18, 19] to be possible feedforward controllers (compensators) structure for additive structured models that contain hysteresis or other types of nonlinearities. In this paper, as shown in Fig.3 and characterized by Eq.6, the model itself has an inverse multiplicative structure. Applying the dual idea of [16, 17, 18, 19], let us suggest an additive structured compensator for the inverse multiplicative structured model. The compensator is displayed in Fig.4(a) where θ_d is the new input. As from the figure, relative to the model to be compensated for, the compensator is direct multiplicative structure but relative to itself it has an additive structure. This feedforward control will result in the linear model of Fig.4(b) where $[g]$ is a static gain around unity and supposed to be uncertain in order to account for possible non-exactitude of the compensation, that is $[g] = [1 - \varepsilon_g, 1 + \varepsilon_g]$, for $\varepsilon_g > 0$. This uncertainty $[g]$ can be rewritten as a direct multiplicative structure relative to a nominal model G_o as displayed in Fig.4(c) and which includes a normalized parametric uncertainty Δ_n (i.e. $-1 \leq \Delta_n \leq 1$) and a weighting $W_\Delta = \varepsilon_g$.

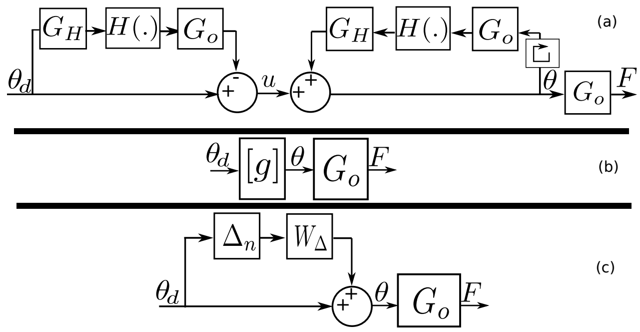

Fig. 4. Feedforward control. (a): with the compensator. (b): equivalent result. (c): equivalent result with direct multiplicative structured uncertainty.

The linear model of Fig.4(c) which contains a direct multiplicative structured uncertainty will be used in the next subsections to calculate a feedback controller. We propose to use the standard H_∞ approach. It allows to account for prescribed desired performances during the design and to satisfy them in the presence of uncertainty.

3.2 Specifications for the feedback

We first remind the specifications desired for the closed-loop:

- tracking performances specification: we desire that the step-response of the closed-loop be without oscillation, has a settling time less than $0.1s$ and a static error less than 1%;
- command moderation specification: we desire that the driving voltage $u(t)$ do not exceed $85V$ when the reference force ranges up to $10N$. This is equivalent to bound the new input θ_d by approximately $85[V] \cdot G_o(0) \cdot G_H(0) = 85[V] \cdot \frac{(k_1+k_2)}{k_2} = 100[V]$.
- noise rejection specification: the force sensor for the feedback is with noise and we would like to attenuate its effect to the driving command θ_d. We assume that the noise starts from $125[rad/s]$.
- robust performances: finally, we would like that the above three specifications be satisfied even in presence of the normalized parametric uncertainty Δ_n weighted by W_Δ.

3.3 Feedback controller synthesis

From the specifications in Subsection.3.2, the augmented closed-loop scheme is constructed. This yields Fig.5(a) where $C(s)$ is the controller to be designed, and $W_\epsilon(s)$, $W_\theta(s)$ and $W_n(s)$ are the weightings for the tracking performances, the command moderation and the noise rejection specifications respectively. Knowing the robust stability condition when having a closed-loop with a direct mutliplicative structured uncertainty (i.e. $\|G_o \cdot C \cdot S \cdot W_\Delta\|_\infty < 1$), Fig.5(a) is equivalent to Fig.5(b) for a standard H_∞ design purpose. A standard scheme is thus derived as shown in Fig.5(c) where o_ϵ, o_θ and o_Δ are the weighted outputs (controlled outputs); F_d and i are the exogeneous inputs; and $P(s)$ is called augmented system.

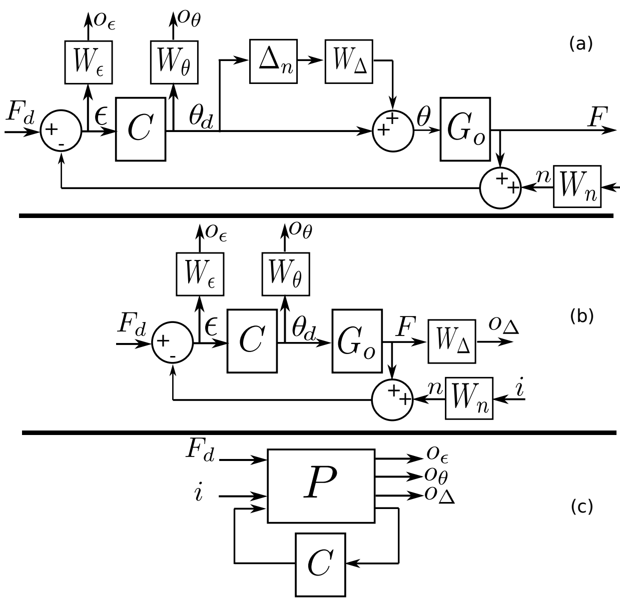

Fig. 5. Feedback controller design. (a): consideration of the specifications. (b): equivalent scheme. (c): the standard scheme.

Problem 1. (Standard H_∞ problem, [20]). The target consists in finding the controller $C(s)$ such that:

. the interconnection represented by the standard scheme in Fig.5(c) be internally stable,

. and $\|LFT_l\,(P,C)\|_\infty < \gamma$.

where $LFT_l\,(P,C)$ is the lower linear fractional transformation of the standard scheme in Fig.5(c) such that:

$$\begin{pmatrix} o_\varepsilon \\ o_\theta \\ o_\Delta \end{pmatrix} = LFT_l\,(P,C) \cdot \begin{pmatrix} F_d \\ i \end{pmatrix} \tag{7}$$

From Fig.5(b) however, we have the following equations:

$$\begin{cases} o_\varepsilon = W_\varepsilon S - W_\varepsilon S W_n \\ o_\theta = W_\theta CS - W_\theta CSW_n \\ o_\Delta = W_\Delta G_o CS - W_\Delta G_o CSW_n \end{cases} \tag{8}$$

where $S = (1+G_oC)^{-1}$ is the sensitivity function. Hence:

$$LFT_l\,(P,C) = \begin{pmatrix} W_\varepsilon S & -W_\varepsilon SW_n \\ W_\theta CS & -W_\theta CSW_n \\ W_\Delta G_o CS & -W_\Delta G_o CSW_n \end{pmatrix} \tag{9}$$

Therefore, from Eq.9, Problem.1 is equivalent to finding the feedback controller $C(s)$ such that:

$$\begin{pmatrix} \|W_\varepsilon S\|_\infty < \gamma & \|-W_\varepsilon SW_n\|_\infty < \gamma \\ \|W_\theta CS\|_\infty < \gamma & \|-W_\theta CSW_n\|_\infty < \gamma \\ \|W_\Delta G_o CS\|_\infty < \gamma & \|-W_\Delta G_o CSW_n\|_\infty < \gamma \end{pmatrix} \tag{10}$$

A classical and practical way to solve the latter problem consists in finding the controller $C(s)$ such that the following conditions hold:

$$\begin{pmatrix} |S| < \gamma \left|\frac{1}{W_\varepsilon}\right| & |S| < \gamma \left|\frac{1}{W_\varepsilon W_n}\right| \\ |CS| < \gamma \left|\frac{1}{W_\theta}\right| & |CS| < \gamma \left|\frac{1}{W_\theta W_n}\right| \\ |G_oCS| < \gamma \left|\frac{1}{W_\Delta}\right| & |G_oCS| < \gamma \left|\frac{1}{W_\Delta W_n}\right| \end{pmatrix} \tag{11}$$

where $\frac{1}{W_\epsilon}$, $\frac{1}{W_\epsilon W_n}$, $\frac{1}{W_\theta}$, $\frac{1}{W_\theta W_n}$, $\frac{1}{W_\Delta}$ and $\frac{1}{W_\Delta W_n}$ are called frequency domain bounds. These bounds are obtained from the specifications. Specifically, $\frac{1}{W_\epsilon}$ is a direct transcription of the tracking performances specification, $\frac{1}{W_\theta}$ is for the command moderation specification, $\frac{1}{W_\theta W_n}$ is for the noise rejection specification, and $\frac{1}{W_n}$ is the uncertainty bound already defined previously. In the next subsection, Structures and numerical values of these bounds will be given.

Note that to solve the problem in Inequations.10, we use the Glover-Doyle (or DGKF) algorithm which is based on the Riccati equations [21, 22].

3.4 Weightings derivation

From the tracking performances specification in Subsection. 3.2, the following bound is used:

$$\frac{1}{W_\epsilon(s)} = \frac{k_{ovs-\epsilon}s + \frac{3\epsilon_{s-\varepsilon}}{t_{set-\epsilon}}}{s + \frac{3}{t_{set-\epsilon}}} = \frac{s+0.2727}{s+27.27} \tag{12}$$

where $k_{ovs-\epsilon}$ is related to the desired maximal overshot, $\epsilon_{s-\varepsilon}$ is the desired maximal static error and $t_{set-\epsilon}$ is the desired maximal settling time. The weighting W_ϵ is thus deduced: $W_\epsilon = \frac{s+27.27}{s+0.2727}$.

From the command moderation specification in Subsection. 3.2, we propose the following bound and thus the weighting:

$$\frac{1}{W_\theta(s)} = \frac{100[V]}{10[N]} \Rightarrow W_\theta(s) = 0.1[N/V] \tag{13}$$

Finally, from the noise rejection specification, the following structure of bound is given:

$$\frac{1}{W_\theta(s)\cdot W_n(s)} = \frac{10/w_{cn}s + \epsilon_{s-n}}{1/w_{cn}s+1} \tag{14}$$

where $\epsilon_{s-n} = \frac{1[V]}{0.1[N]}$ is the chosen noise rejection at low frequency and $w_{cn} = 126[rad/s]$ is the chosen cutting frequency. This yields a weighting: $W_n(s) = 1$.

3.5 Feedback controller derivation

Using the numerical values in Table.1, the weightings in Subsection.3.4, and applying the Glover-Doyle algorithm to Inequations.10 with MATLAB, we obtain an optimal controller of order 3:

$$\begin{cases} C(s) = \frac{2867\left(s^2+9.179s+123.8\right)}{(s+0.2727)(s^2+15.4s+155.5)} \\ \gamma_{opt} = 1.67 \end{cases} \tag{15}$$

where the optimal performance level γ_{opt} is close to unity which permits to predict that the specifications will be (almost) satisfied. Note that the controller order ($= 3$) is lower than the order of the nominal system $G_o(s)$ ($= 4$) added with the total order of the weightings ($= 1$). In fact, when replacing the coefficients of the model $G_o(s)$ with their numerical values, two stable poles are almost equal to two zeros and thus vanish. The model used by the controller design is therefore of order 2 and the order of the resulting controller is hence justified.

Using the calculated controller, the magnitudes of S, of CS and of G_oCS are compared with the bounds $\frac{1}{W_\epsilon}$, $\frac{1}{W_\theta}$, $\frac{1}{W_\theta W_n}$ and $\frac{1}{W_\Delta}$. Fig.6 displays the results which reveal that the conditions given in Inequations.10 are satisfied.

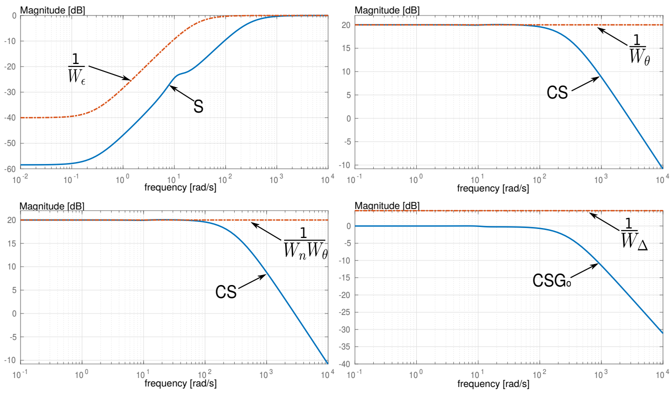

Fig. 6. Magnitudes of the bounds and of the closed-loop transfers.

4. SIMULATION AND DISCUSSIONS

This section presents the application of the calculated feedforward-feedback control law to the robot of Fig.2. The implementation is displayed in Fig.7. The simulation results are presented.

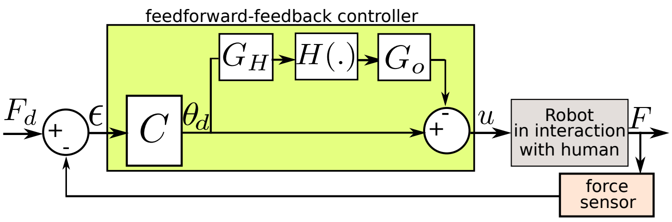

Fig. 7. Implementation diagram.

4.1 Feedforward control results

The feedforward control scheme of Fig.4(a) is first tested. In all the simulation, the Prandtl-Ishlinskii hysteresis model [23] is used as $H(\cdot)$. However the hysteresis operator that we use in the compensator is expressly put slightly different from that of the model in order to have a non-exact compensation. The resulting (θ_d, θ)-map, for different conditions (excitation frequency in particular) is displayed in Fig.8 where we observe the gain not exactly equal to unity due to the non-exact compensation, and different according to the excitation frequency. This non-unity and variability of the gain will be considered as uncertainty in the sequel by using the uncertainty modeling in Subsection.3.1.

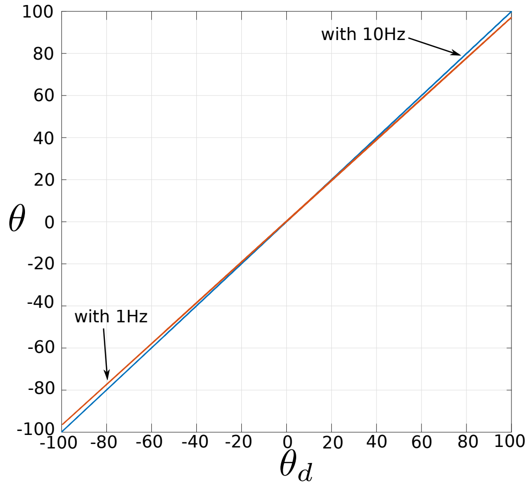

Fig. 8. Feedforward control results.

4.2 Feedforward-feedback control results

The calculated H_∞ controller in Subsection.3.5 is added to the feedforward controller. First, the step response of the entire closed-loop is verified. Though a step input will not be used in the human-robot interaction for safety reason, here the aim is to verify the tracking performances. Fig.9 displays the result when a step reference of $F_r = 10N$ is applied. It reveals that the closed-loop is much more performant than the bound $\frac{1}{W_\epsilon}$. Indeed, the step-response of the closed-loop has a settling time of $13ms$, zero overshot and a static error less than 1%, which are much better than those of the bound.

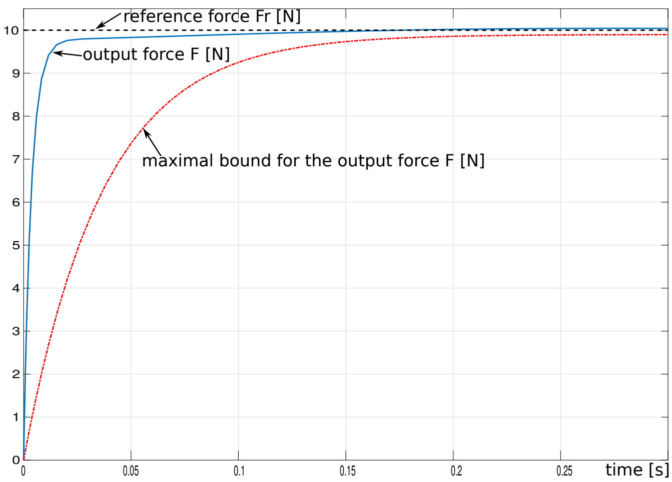

Fig. 9. Step response of the closed-loop.

Then, a sine input reference with $10N$ of amplitude and $0.1Hz$ of frequency is applied. Fig.10(a), (b) and (c) illustrate the tracking result, the tracking error and the input-output map respectively. They indicate interesting reference tracking with an error less than $\frac{0.1[N]}{10[N]} = 1\%$.

In order to check the trajectory tracking performance at higher frequency, we apply a sine reference at $1Hz$ to the closed-loop. Fig.11(a), (b) and (c) provide the results. Fig.11(c) particularly indicates that a phase lag starts to appear. Meanwhile, all the figures show that the output amplitude still remains convenient and the error less than

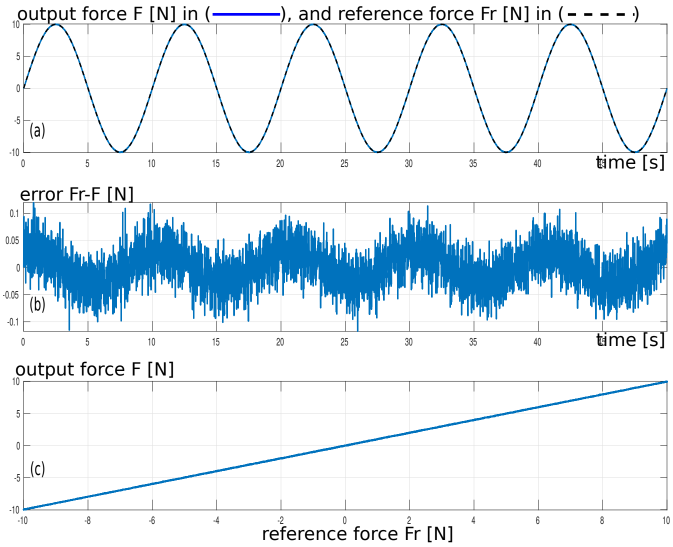

Fig. 10. Sine trajectory tracking response with $f = 0.1Hz$.

$\frac{0.4}{10} = 4\%$. For higher frequency of the input reference, for instance $5Hz$ and $10Hz$, the phase-lag increases but the output amplitude still remains high as Fig.12 shows (a and c for $5Hz$ and b and d for $10Hz$). In fact, from the complementary sensitivity $1-S$, the bandwidth of the closed-loop is evaluated at $44Hz$ from which the output amplitude starts to decrease substantially.

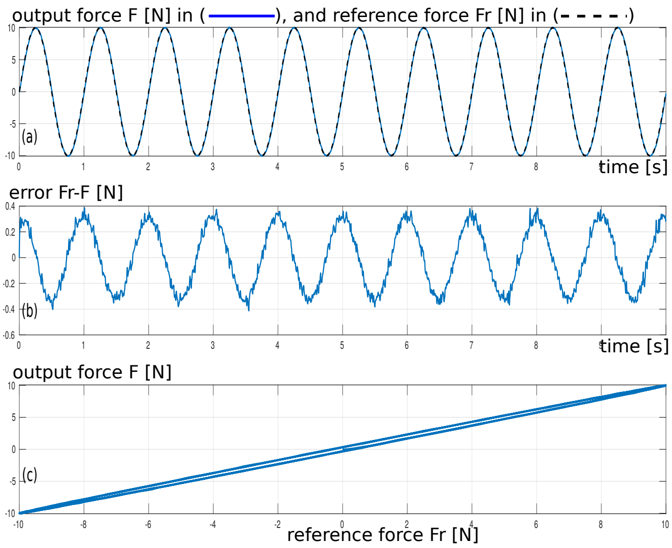

Fig. 11. Sine trajectory tracking response with $f = 1Hz$.

Finally, a combination of several sines is used as reference and is applied to the closed-loop: $F_r(t) = 10N \cdot \sin(2 \cdot \pi \cdot 0.1Hz) + 5N \cdot \sin(2 \cdot \pi \cdot 1Hz) + 2.5N \cdot \sin(2 \cdot \pi \cdot 5Hz)$. Fig.13(a) and (b) display the time-domain response and the input-output map which still reveal good tracking performances.

4.3 Discussions

The different simulation results presented above demonstrate the efficiency of the proposed feedforward-feedback control of a one-dof robot in interaction with a human. An assumption made in the human model, and thus affected the controllers design, is the fact that the human does not

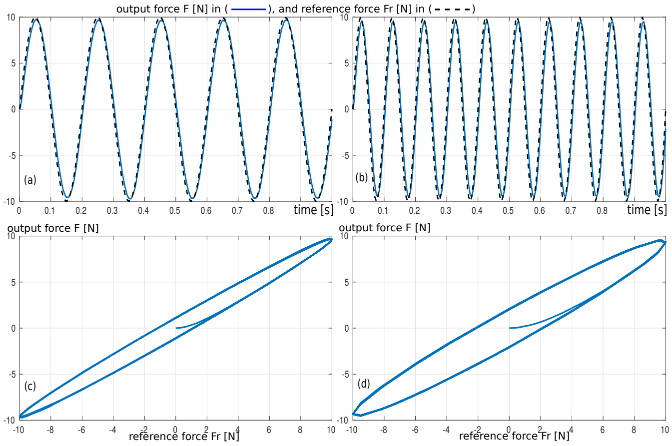

Fig. 12. Sine trajectory tracking response with higher frequencies ($f = 5Hz$ and $10Hz$).

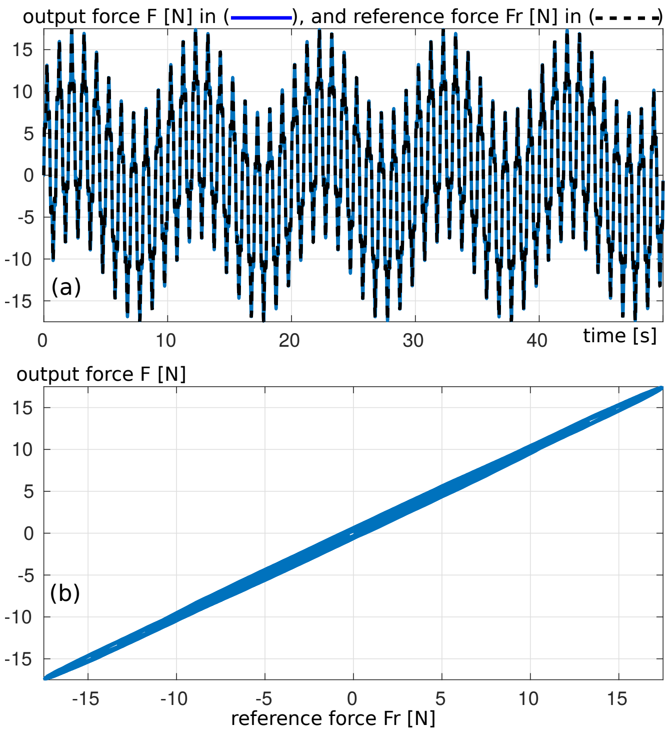

Fig. 13. Complex trajectory tracking response.

deliberately generates force. This assumption might not correspond to the reality for certain applications such as robotics for sport and training. In such case, the force deliberately generated by the human could be considered as external disturbance to be considered during the feedback controller synthesis.

The reference input F_r used during the simulation has sine shape. In real situation, the trajectory could be different. For more complex signal shape or for frequency higher than the bandwidth $44Hz$, it might be recommended to take into account the reference signal type during the feedback controller design.

The results reported in this paper were from simulation. When experimented, the closed-loop might result in slightly degraded performances. However, as from the specifications and closed-loop results comparison displayed in Fig.6(a) and in Fig.9, the margin from the bound is sufficiently large and consequently the acceptable margin of degradation is still large.

Finally, one necessary condition to allow the experimental work is the availability of force sensor. However standard sensors in robotics might affect the overall model if placed between the human feet and the end-effector of the robot due to their non-ngegligible mass and size. A perspective we are working on is the use of thin-films based piezoelectric materials. Preliminary works demonstrate that such materials can be used as sensors additionally to other functions they can provide [24, 25].

5. CONCLUSIONS

This paper presented the control of a human-robot interaction for applications such as relaxing exercise, or for massage. While a nonlinear model is used for the human, a feedforward combined with a feedback scheme is used for the control. First the feedforward controller is employed to compensate for the nonlinearity. Then the feedback which is based on the H_∞ technique is used to add robustness against possible uncertainties and to satisfy desired performances. Extensive simulation were carried out and demonstrated the efficiency of the proposed control technique. Ongoing works consist in verifying the control techniques with an experimental benchmark based on a robotized system actuated with a linear motor. Furthermore, expected perspective consists in using a 6-dof robot as well instead instead of the 1-dof robot.

REFERENCES

[1] A. S. Al-Yahmadi, J. Abdo, and T.C. Hsia. Modeling and control of two manipulators handling a flexible object. *J of the Franklin Institute*, 344(5), 2007.

[2] D. Sun, J. K. Mills, and Y. Liu. Position Control of Robot Manipulators Manipulating a Flexible Payload. *The International Journal of Robotics Research*, 18(3):319–332, 1999.

[3] B. Esakki, R. B. Bhat, and C-Y. Su. Robust control of collaborative manipulators - flexible object system. *Int J. of Advanced Robotic Systems*, 10(5):257, 2013.

[4] D. Heirich and H. Wörn, editors. *Robot Manipulation of Deformable Objects*. Springer, 2000.

[5] S. Flixeder, T. Glück, and A. Kugi. Modeling and force control for the collaborative manipulation of deformable strip-like materials. *IFAC-PapersOnLine*, 49(21):95–102, 2016.

[6] D. Navarro-Alarcon et al. Automatic 3-d manipulation of soft objects by robotic arms with an adaptive deformation model. *IEEE Transactions on Robotics*, 32:429–441, 2016.

[7] P. Donner et al. Cooperative Dynamic Manipulation of Unknown Flexible Objects Joint Energy Injection Based on Simple Pendulum Fundamental Dynamics. *Int Journal of Social Robotics*, 9(4):575–599, 2017.

[8] F. F. Khalil and P. Payeur. Dexterous Robotic Manipulation of Deformable Objects with Multi-Sensory Feedback - a Review. In *Robot Manipulators Trends and Development*, pages 587–622. 2010.

[9] F. Nadon, A. Valencia, and P. Payeur. Multi-Modal Sensing and Robotic Manipulation of Non-Rigid Objects: A Survey. *Robotics*, 7(4), 2018.

[10] J. Sanchez et al. Robotic manipulation and sensing of deformable objects in domestic and industrial applications: a survey. *Int J. of Robotics Research*, 37(7):688–716, 2018.

[11] F. Ruggiero et al. Nonprehensile Manipulation of Deformable Objects: Achievements and Perspectives from the Robotic Dynamic Manipulation Project. *IEEE Robotics Automation Mag*, 25(3):83–92, 2018.

[12] Y. Yamakawa et al. Toward Dynamic Manipulation of Flexible Objects by High-Speed Robot System. In *Dynamic Modelling and Control of Robotic Interaction*. Intechopen edition, 2018.

[13] P. Long, W. Khalil, and P. Martinet. Force/vision control for robotic cutting of soft materials. *2014 IEEE/RSJ International Conference on Intelligent Robots and Systems*, pages 4716–4721, 2014.

[14] J. Mizrahi and Z. Susak. In-yivo elastic and damping response of the human leg to impact forces. *Journal of Biomechanical Engineering*, 104(1):63–66, 1982.

[15] V. Bonnet et al. A closed loop musculoskeletal model of postural coordination dynamics. *Conference on Decision and Control*, pages 6207–6212, Dec 2009.

[16] M. Rakotondrabe. Bouc-wen modeling and inverse multiplicative structure to compensate hysteresis nonlinearity in piezoelectric actuators. *IEEE Trans on Automation Science and Eng*, 8(2), 2011.

[17] M. Rakotondrabe. Modeling and compensation of multivariable creep in multi-dof piezoelectric actuators. *IEEE International Conference on Robotics and Automation*, pages 4577–4581, 2012.

[18] M. Rakotondrabe. Multivariable classical prandtl-ishlinskii hysteresis modeling and compensation and sensorless control of a nonlinear 2-dof piezoactuator. *Nonlinear Dynamics*, 2017.

[19] D. Habineza, M. Rakotondrabe, and Y. Le Gorrec. Multivariable generalized bouc-wen modeling, identification and feedforward control and its application to a 2-dof piezoelectric multimorph actuator. *IFAC WC*, pages 10952–10958, 2014.

[20] G. J. Balas, J. C. Doyle, K. Glover, A. Packard, and R. Smith. -analysis and synthesis toolbox. *The Mathworks User's Guide-3*, 2001.

[21] K. Glover and J. C. Doyle. h_∞-norm bound and relations to risk sensivity. *Systems & Control Letters*, 11:167–1721, 1988.

[22] J. C. Doyle, K. Glover, P. K. Khargonekar, and B. A. Francis. State-space solutions to standard h_2 and h_∞ control problems. *IEEE Transactions on Automatic Control*, 34(8):831–846, 1989.

[23] M Al Janaideh, M Rakotondrabe, I Al-Darabsah, and O Aljanaideh. Internal model-based feedback control design for inversion-free feedforward rate-dependent hysteresis compensation of piezoelectric cantilevered actuator. *Control Eng. Practice*, 72:29–41, 2017.

[24] M. Rakotondrabe. Combining self-sensing with an unkown-input-observer to estimate the displacement, the force and the state in piezoelectric cantilevered actuator. *American Control Conference*, pages 4523–4530, 2013.

[25] O. Aljanaideh and M. Rakotondrabe. Observer and robust h-inf control of a 2-dof piezoelectric actuator equiped with self-measurement. *IEEE RAL*, pages 1080–1087, 2018.